LAWRENCE
LIVERMORE
NATIONAL
LABORATORY

LLNL-JRNL-575474

Branching Mechanisms in Surfactant Micellar Growth

M. Tang, W. C. Carter

August 21, 2012

Journal of Physical Chemistry B

Disclaimer

Branching Mechanisms in Surfactant Micellar Growth

Ming Tang[1,*] and W. Craig Carter[2]

[1]*Lawrence Livermore National Laboratory, Livermore, CA 94550 USA*

[2]*Massachusetts Institute of Technology, Cambridge, MA 02139 USA*

Abstract

We present a phase-field model to study the morphological transitions of surfactant micelles in supersaturated dilute solution. Simulations reveal that multiply connected micellar structure can be produced by interface branching instability of a growing micelle at relatively large supersaturation and intermediate spontaneous curvatures. Two branching mechanisms, i.e. a disk–to–cylinder shape transition and a tip bifurcation process, are identified for disklike and cylindrical micelles, respectively. We propose that dynamic branching at the micelle growth front provides an important kinetic pathway for the formation of branched wormlike micelles that are observed in many surfactant systems.

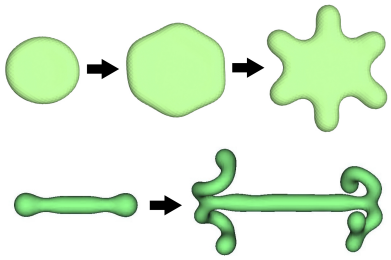

Keywords: branched wormlike micelles, dynamic branching mechanisms, micelle morphological transitions, interface instability, phase–field simulation, linear stability analysis

At sufficiently large concentrations, amphiphilic molecules such as surfactants can form micellar structures in solutions with three characteristic morphologies: sphere, cylinder, and bilayer. Micelle morphology derives from the bending curvature energy of surfactant layers with an expression introduced by Helfrich [1]: $E_{curv} = \iint dA\,[2\kappa(H - H_0)^2 + \overline{\kappa}K]$. H and K are the mean and Gaussian curvatures of the surfactant layers, and κ and $\overline{\kappa}$ are their corresponding bending moduli. The spontaneous curvature H_0 is an intrinsic property of the surfactant/solvent system that originates from the volume difference between the head- and tail-groups, and is influenced by parameters such as temperature, electrolyte, and co-surfactants. As H_0 increases, different equilibrium micelle shapes are produced that vary from bilayer to cylindrical and then to spherical morphologies.

However, other micelle morphologies with non-constant curvatures are also observed; in particular, experiments reveal the existence of "branched wormlike" micellar networks [2–4], in which multiple elongated cylinder segments are interconnected by threefold "Y-shaped" junctions (e.g. see Fig. 1(a) of ref. [5]). The development of branch points among cylindrical micelles has significant impact on the rheological properties [6, 7] and phase stability of the surfactant solutions [3]. Because the junctions have very different curvatures from the cylindrical body, their thermodynamic stability and that of the branching network have been extensively studied [5, 8, 9]. However, the processes by which branches form and evolve is less understood.

Branched wormlike micelles are reminiscent of snow flakes, ramified trees, river deltas and many other branched structures found in nature. In many cases, dynamic instability of growth fronts produces branching such as in dendritic growth [10] and viscous fingering [11]. Here we use phase-field simulations to show that similar interface instability also occurs during micellar growth and can lead to the formation of branched morphology.

The phase-field method has provided considerable insights to dendritic growth [10, 12] and other microstructure evolution phenomena in materials [13]. We recently developed a phase-field model for micellar growth in dilute solutions [14]. The model is briefly described below. Details can be found in ref. [14]. In a surfactant/polar solvent binary system, a scalar phase-field variable $\phi(\vec{x})$ is introduced to characterize local surfactant concentration and distinguish between the micelle "phase" and the liquid phase. $\phi(\vec{x})$ varies smoothly along a spatial trajectory from -1 at the hydrophobic micelle core to $\phi_{sol} \approx 1$ in solution, where (1-ϕ_{sol})/2 represents the volume fraction of free surfactants in solution. The head

groups of surfactants are assumed to always abut the polar solvent at the micelle/solution interface specified by the level surface $\phi(\vec{x}) = 0$. The following free energy functional for $\phi(\vec{x})$ is proposed

$$F[\phi(\vec{x})] = \iiint \left[f(\phi) + \frac{\lambda\sigma^2}{2} p(\phi)^2 - 4\lambda H_0 \left|\nabla\phi\right| \nabla^2\phi \right.$$
$$\left. + \left(\frac{\nu(\phi)}{2} + \lambda\sigma p'(\phi) + 2\lambda H_0^2 \right) \left|\nabla\phi\right|^2 + \frac{\lambda}{2} (\nabla^2\phi)^2 \right] dV \tag{1}$$

By rewriting Eq. 1 in a local orthogonal coordinate system (r,s,t), where r runs in the direction of $\nabla\phi$ and s and t lie in the local tangent plane of the ϕ level surfaces, we show [14] that F can be divided into two parts, i.e. $F = F_{curv} + F_{chem}$. F_{curv} is the the curvature-related energy contribution

$$F_{curv} = \iiint dV \lambda \left(\frac{\partial\phi}{\partial r} \right)^2 \left[2(H(\vec{x}) - H_0)^2 - K(\vec{x}) \right] \tag{2}$$

where $H(\vec{x})$ and $K(\vec{x})$ are the mean and Gaussian curvatures of the level surface of ϕ at point $\vec{x}$=(r,s,t). In the sharp-interface limit Eq. 2 reduces to a surface integral over the micelle/solution interface and recovers the Helfrich curvature energy expression where the bending moduli are: κ=-$\overline{\kappa}$=$\lambda \int (\partial\phi/\partial r)^2 dr$.

The curvature-independent part of the free energy is

$$F_{chem} =$$
$$\iiint dV \left[f(\phi) + \frac{\nu(\phi)}{2} \left(\frac{d\phi}{dr} \right)^2 + \frac{\lambda}{2} \left(\frac{\partial^2\phi}{\partial r^2} - \sigma p(\phi) \right)^2 \right] \tag{3}$$

where $p(\phi)$=$1/16(1-\phi)^3(8+9\phi+3\phi^2)$ interpolates smoothly between $p(-1) = 1$ and $p(1) = 0$. $f(\phi)$ in Eq. 3 is the homogeneous chemical free energy density. It is modeled by a double-well-shaped piece-wise polynomial with two minima at $\pm\phi_m \approx \pm 1$ to reflect the immiscibility between surfactant and solvent. The "emulsion behavior" of the surfactant solution has been modeled by a concentration-dependent gradient coefficient $\nu(\phi)$=$\nu_0 + (\nu_1 - \nu_0)\phi^2$ with $\nu_0 < 0$ and $\nu_1 > 0$ [15]. The negative values of ν near the interface ϕ=0 causes the interface area to spontaneously grow, i.e., to expose as many head groups to the solvent as possible, and a positive $\nu(\phi$=1) for the solvent ensures the stability of the bulk solution. It can be shown that the λ-dependent term in Eq. 3 introduces the surfactant layer-layer interaction that stabilizes a bilayer structure with an equilibrium (self–assembly) thickness $l_0 \propto \sigma^{-1/2}$ [14]. Therefore both the self-assembly behavior of surfactants in solvent and the bending curvature energy of

surfactant layers are captured in Eq. 1. We note that Eq. 1 is similar to the Ginzburg–Landau formulation developed by Gompper and coworkers for oil/water/amphiphile ternary systems [15], but the spontaneous curvature and micelle length scales are explicitly incorporated in our model. The free energy form of our model also shares features with the phase-field crystal theory [16] which includes a trade-off between negative and positive gradient energy terms that produces a "self-assembly" of ensemble-averaged atoms into crystalline structures.

The time evolution of ϕ is postulated to follow the Cahn-Hilliard equation [17] for conserved order parameters:

$$\partial\phi/\partial t = M\nabla^2(\delta F/\delta\phi) \tag{4}$$

where M is the mobility of surfactants in solution. Eq. 4 is used to simulate micellar growth with a spectral method after non-dimensionalizing Eqs. 1 and 4 with length, energy and time units l_c=2 nm, ϵ_c=2.5×10^{-18} J and t_c=$M\epsilon_c/l_c^3$. Parameters in Eq. 1 can be fitted to the properties of a specific surfactant/solvent system. In all simulations presented here, dimensionless parameters ϕ_m=0.999, σ=15, ν_0=-0.075, ν_1=0.001, and λ=0.005 are used. They produce a critical micelle concentration of 0.05% volume fraction, bilayer half thickness $l_0\approx$ 2 nm, and bending stiffness $\kappa\approx$ 20 kT, which are similar to the properties of short-chain surfactants like cetyltrimethylammonium bromide (CTAB) in which branched micelles were found to form at increased salt concentrations [6]. Nevertheless, we systematically varied the value of H_0 in simulations to examine the effects of spontaneous curvature on micellar growth morphology.

We simulated the growth of a spherical micelle nucleus in a supersaturated surfactant solution. The initial concentration of the solution was slightly perturbed from a uniform value. A 64×64×64 mesh with grid spacing $\Delta x = 10/64$ and periodic boundary conditions was used. (all physical units refer to their non-dimensionalized form as described above.) At an initial concentration $c_0 = 2\%$ volume fraction, the growing micelle's morphology varies from spherical to cylindrical to disklike as H_0 is decreased from $1/l_0$ to $1/2l_0$ and to 0, as shown in Fig. S1 in the Supporting Information. which conforms to predictions from the curvature energy model. Upon increasing supersaturation, however, new micelle growth behavior emerges. We illustrate this by setting $H_0 = 0.25$—which is intermediate to cylindrical and disk-like forms—and comparing micelle evolution behavior at concentration $c_0 = 2\%$, 3% and 4% as shown in Fig. 1 and the Supporting Information. For $c_0 = 2\%$, the nucleus grows into a cylindrical micelle. At $c_0 = 3\%$, however, a disklike micelle emerges

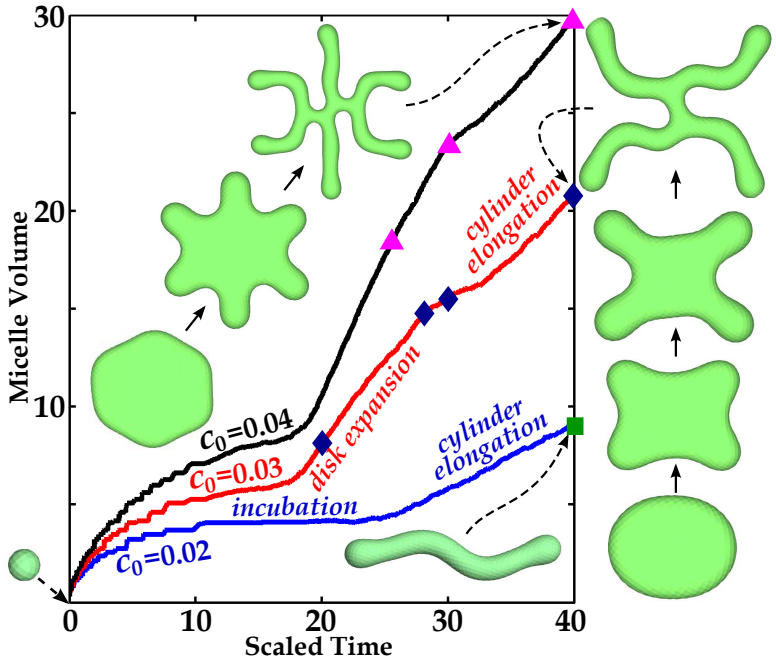

FIG. 1: Snapshots of the ϕ=0 level surface of a micelle growing from a spherical nucleus in solution of c_0 = 2%, 3% and 4%, superimposed on the micelle volume-vs-time curves. The times the snapshots correspond to are marked by ■ for c_0=2%, ♦ for c_0=3% and ▲ for c_0=4%.

from the nucleus growth with its radius increasing with time. Nevertheless, the disk's rim becomes unstable at large radii. As shown in Fig. 1, perturbation develops at the growth front and generates four finger–like protuberances around t=28 that subsequently grow by consuming volume from the disk's bilayer region. Eventually, the disklike micelle is transformed into a multi–connected cylindrical micelle with individual arms linked by two threefold junctions: a morphology that bears close resemblance to the branched worm-like micelles observed in experiments. Fig. 1 also shows the time dependence of micelle volume upon micellar growth. The relatively constant slopes of the micelle volume growth curve in both the disk expansion and cylinder elongation regimes suggest that the disk radius grows as $t^{1/2}$ and the subsequently formed cylindrical branches lengthen at a steady state. A similar morphological transition sequence is also seen at the higher supersaturation c_0 = 4%. Nevertheless, the disk shape instability develops at larger radii with more (six) arms formed at the growth front, producing a branched micelle with four junctions.

This disk–to–cylinder transition behavior (e.g. at $c_0 = 3\%$) persists even as H_0 is increased to 0.5 which strongly favors the cylindrical morphology. However, unlike the the case of

$H_0 = 0.25$, for $H_0 = 0.5$, the initially formed branch points become unstable and break up at a later time, resulting in a final configuration of disconnected cylindrical micelles (see Fig. S2 in the Supporting Information). Therefore, our simulations reveal that two independent conditions are necessary for producing stable branched micelles: 1) an intermediate H_0 between those preferring the disk and cylinder morphologies, and 2) a sufficiently large surfactant supersaturation. They are consistent with the experimental observations that a morphological transition from linear to branched wormlike micelles can be induced by increasing surfactant [3] and/or electrolyte concentrations [4, 6] in solution. The latter has the effect of reducing electrostatic repulsion between head groups of ionic surfactants and lowering the effective spontaneous curvature.

Our simulations suggest that the micelle growth morphology is controlled by the interplay between surfactant-supersaturation and the bending curvature energy of surfactant layers. Compared to the one-dimensional growth behavior exhibited at c_0=2% for H_0=0.25 and 0.5, a larger driving force supplied by the increased supersaturation at c_0=3% can overcome the unfavorable curvature-energy and induce a quasi-two-dimensional micelle morphology that facilitates a higher growth rate. However, when free monomers in solution are gradually consumed by disk growth that causes the driving force to drop, the micelle shape will transform back to the preferred cylindrical geometry under the influence of curvature energy. Such a morphological transition is initiated by the growth front instability of disklike micelles, which is analogous to dendritic growth in solidification of crystalline materials **??** but has not been reported before for surfactant micelles. We show below that the onset of micelle shape instability can be explained by a linear stability analysis similar to the classical Mullins-Serkeka instability [18] for a solidifying growth front. To analyze stability, we consider diffusion-limited disklike micelle growth in a two-dimensional system. The disk radius $R \gg l_0$ is initially perturbed by small amplitude wave: $r(\theta)=R+\epsilon\cos(n\theta)$ (n=1,2,3,...), $\epsilon \ll R$. Let c_0 and c_{eq} be the concentrations at infinity and the micelle/solution interface, respectively, and assume that the micelle consists only of surfactant molecules. In the small supersaturation limit $\Delta\overline{C} \equiv (c_0 - c_{eq})/(1 - c_{eq}) \ll 1$, surfactant diffusion in front of the disk can be assumed to be quasi–steady–state and follow the Laplace equation, $\nabla^2 c = 0$. The boundary condition at the micelle/solution interface is given by

$$c_{eq}(\theta) = c_{eq}^0 \left(1 + \frac{\Omega}{2kTl_0 r(\theta)} \frac{\delta \Delta E_{curv}^{rim}}{\delta r(\theta)}\right) \tag{5}$$

c_{eq}^0 is the solution concentration in equilibrium with a flat surfactant bilayer and Ω is the volume of a monomer. Eq. 5 is similar to the Gibbs–Thomson relation and accounts for the increased surfactant chemical potential due to the local excess bending curvature energy of the disk's rim, which is

$$\Delta E_{curv}^{rim} = \frac{\pi\kappa l_0}{2}\int_0^{2\pi}(\varkappa^r - \varkappa_0^r)^2\sqrt{r(\theta)^2 + r'(\theta)^2}d\theta \tag{6}$$

where $\varkappa^r = (r^2 + 2r'^2 - rr'')^2/(r^2 + r'^2)^{3/2}$ is the rim's radial curvature and $\varkappa_0^r \equiv 2H_0 - 1/l_0$ is the preferred radial curvature. On the other hand, the concentration flux at the far-field is determined to be $\partial c/\partial r = 2(c_0 - c_{eq})/|\ln\Delta\overline{C}|r$ from the self-similarity solution of the diffusion equation [10]. By solving the concentration field in solution for these boundary conditions, the disk's growth velocity can be evaluated from the Stefan condition [19]:

$$\frac{dr(\theta)}{dt} = \frac{dR}{dt} + \frac{d\epsilon}{dt}\cos(n\theta) = \frac{D}{1 - c_{eq}}\left.\frac{\partial c}{\partial r}\right|_{r=r(\theta)} \tag{7}$$

We obtain $dR/dt{=}2D/|\ln\Delta\overline{C}|R$ from Eq. 7, which explains the parabolic growth of the disk radius (or the linear growth of the disk volume) seen in Fig. 1. The growth rate of the perturbation amplitude is found to be

$$\begin{aligned}\frac{d\epsilon}{dt} = \frac{D(n-1)}{(1-c_{eq})R} \times \Bigg[&\frac{2(c_0 - c_{eq})}{|\ln\Delta\overline{C}|R} \\ &- \frac{\pi\kappa\Omega c_0}{4kT}\frac{n(n+1)[2n^2 - 3 + (2\varkappa_0^r R)^2]}{R^3}\Bigg]\end{aligned} \tag{8}$$

Note that the first term within the bracket on the right hand side of Eq. 8 scales with R^{-1}, which the second term scales with R^{-3}. Therefore, Eq. 8 shows that for any given wavenumber $n¿1$, a disk micelle will eventually become unstable (i.e. $d\epsilon/dt{>}0$) against the perturbation when its radius R becomes sufficiently large. The critical radius above which the interface instability develops is n- and H_0-dependent. At a given radius, the fastest growing perturbation mode has a wavenumber $n_{\max}{\propto}R^{3/4}$ in a cylinder-favoring system (i.e. $H_0 = 1/2l_0$), or $n_{\max}{\propto}R^{1/2}$ when the bilayer morphology is preferred (i.e. $H_0 \to 0$). The R dependence of $n_{\max}$ explains why more cylindrical fingers emerge from the disk's rim when the initial solution concentration c_0 is increased from 3% to 4% in our simulations (Fig. 1): at the higher supersaturation $c_0{=}4\%$, the disk radius R has a larger growth rate because of the increased driving force. As a result, the growth of perturbation is not significant relative to disk expansion until reaching a larger R, at which the dominant perturbation has a larger wavenumber and more protuberances are thus generated than in the case of $c_0{=}3\%$.

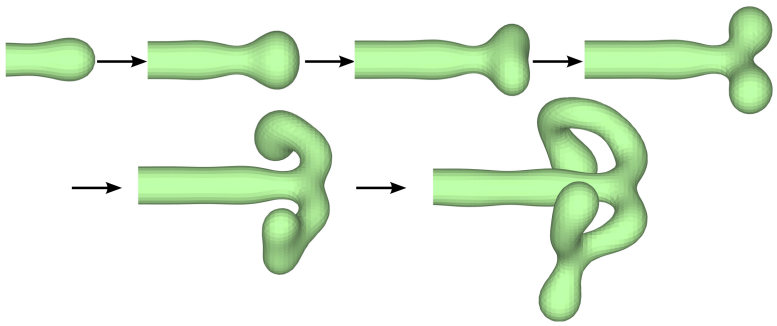

FIG. 2: Snapshots of a cylindrical micelle with H_0=0.25 growing in solution of c_0=3% at t=0, 15, 20, 23, 31 and 36. Only half of the micelle is shown for clarity.

In addition to the disk rim instability, we discovered from simulations that branching can also occur to cylindrical micelles via a tip splitting mechanism. Fig. 2 shows a cylindrical micelle with H_0=0.25 that was first grown from a spherical nucleus at c_0=2%, and subsequently subject to a higher monomer concentration at c_0=3%. After the solution concentration change, the spherical cap of the cylindrical micelle starts to swell because the increased supersaturation causes surfactant monomers to be absorbed into the micelle growth front more rapidly than can be accommodated by the cylinder elongation. However, the larger cap is not favored by the curvature energy, and it gradually flattens and then splits into two smaller caps, leaving a Y–shaped junction behind. The morphological transition consumes surfactant monomers in the region surrounding the cap and reduces the local supersaturation. The newly formed arms thus grow into two cylindrical branches after splitting. As shown in Fig. 2, tip splitting may happen again when the cylinder caps enter regions with sufficiently high surfactant concentration. This phenomenon resembles the tip splitting of a needle crystal in the absence of surface energy anisotropy [10], but here it is the bending curvature energy rather than the surface energy that dampens the interface perturbation. The onset of tip splitting in a cylindrical micelle can be analyzed by a linear stability analysis similar to that for crystal growth [10] and will be reported elsewhere.

The tip bifurcation process provides a mechanism for a single micelle to repeatedly add branch points to itself to sprawl into a hierarchically branched network structure. We demonstrate this point with a micelle growth simulation using H_0=0.25 and c_0 = 3% and a computation domain of size 40×40×40 that is much larger than those used in Fig. 1 and Fig. 2. As shown in Fig. 3, after two junctions emerge from the disk front perturbation of

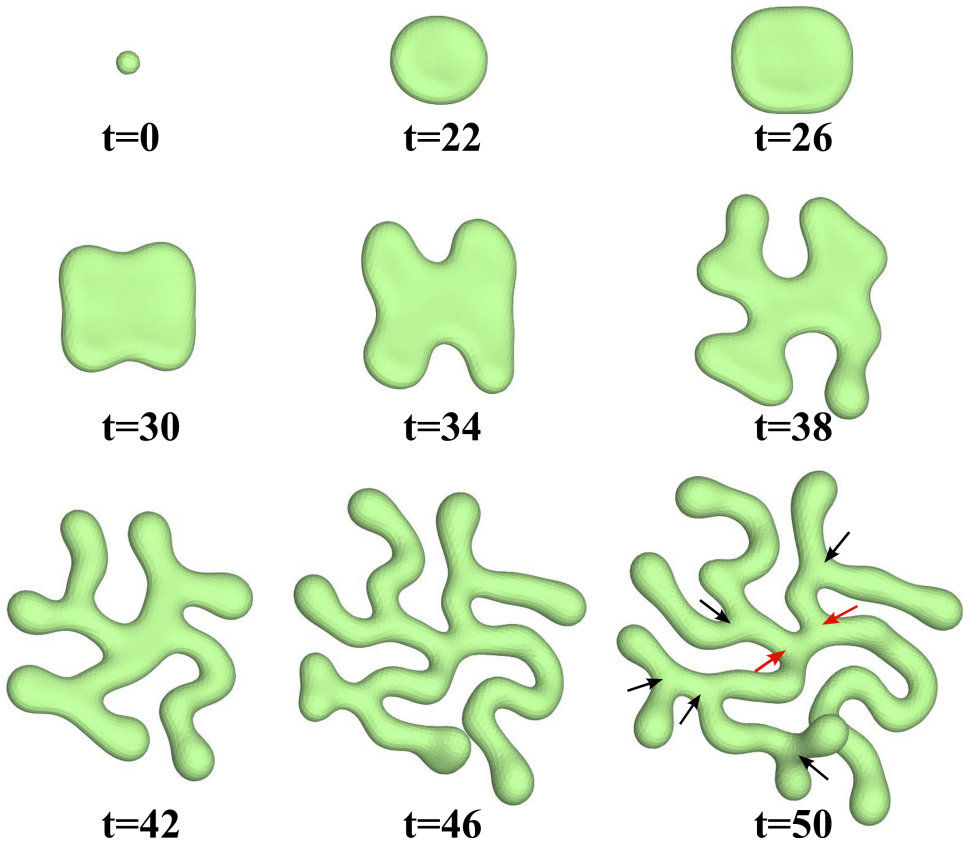

FIG. 3: Snapshots of the ϕ= 0 level surface of a micelle with $H_0 = 0.25$ growing from a spherical nucleus in a solution of $c_0 = 3\%$, using a large computation domain (see text). Branching junctions formed from disk–to–cylinder transition are marked by red arrows and those generated by tip bifurcation are highlighted by black arrows on the micelle snapshot at t=50.

n=4, more junctions are generated by tip bifurcation at the growth front, which result in a multi-connected branched wormlike micelle at the end of simulation. We note that the reason that multiple branching events can occur subsequently in this simulation but not in simulations using smaller domain sizes is that the solution supersaturation decreases more slowly with time upon micellar growth in the larger computation box and the driving force remains sufficiently high for interface instability to develop over an extended period of time.

In conclusion, results from phase-field simulations and linear stability analysis provide the first evidence that links the development of branched wormlike micelles to micelle/solution interface instability during micellar growth. Branch points can develop through disk–to–cylinder or tip–splitting morphological transitions, which lead to the formation of multiply connected network structures. In micellar systems, the equilibrium between micelles

and the surrounding solution is dynamically maintained through constant exchange of surfactant molecules between them. Surfactant monomer concentration in the solution exhibits significant fluctuation both spatially and temporally, and branching instability can occur to micelles in regions with large local supersaturation. While the stability of the as–formed junctions is ultimately determined by the thermodynamic properties of the surfactant/solvent systems, the dynamic branching phenomena revealed in this work provide an important kinetic mechanism for establishing the equilibrium junction density in the micellar networks. Despite recent progress in experimental techniques [2–4, 6, 7] that have considerably enriched our knowledge of branched micelle structures, it remains a challenging task to infer the details of branching dynamics from experimental observations. We demonstrate in this paper that phase-field simulation is a useful tool to compliment experiments to provide valuable insights on the morphological evolution of surfactant self-assembled structures.

Supporting Information: Includes additional figures of micelle morphology formed under different solution concentration and spontaneous curvature and animations of phase-field simulations of micelle branching process.

MT acknowledges financial support from the Lawrence Postdoctoral Fellowship under the auspices of the US Department of Energy by Lawrence Livermore National Laboratory under Contract DE-AC52-07NA27344. Part of the simulations were carried out at the National Energy Research Scientific Computing Center, which is supported by the Office of Science of the U.S. Department of Energy under Contract No. DE-AC02-05CH11231.

* Electronic address: tang25@llnl.gov

[1] W. Helfrich, Z. fur Naturf. C **28**, 693 (1973).

[2] D. Danino *et al.*, Science **269**, 1420 (1995).

[3] A. Bernheim-Groswasser, R. Zana, and Y. Talmon, J. Phys. Chem. B **104**, 4005 (2000).

[4] V. Croce *et al.*, Langmuir **19**, 8536 (2003).

[5] T. Tlusty, S. A. Safran, and R. Strey, Phys. Rev. Lett. **84**, 1244 (2000).

[6] A. Khatory *et al.*, Langmuir **9**, 1456 (1993); C. Oelschlaeger *et al.*, Langmuir **26**, 7045 (2010).

[7] M. In *et al.*, Phys. Rev. Lett. **83**, 2278 (1999).

[8] T. Tlusty and S. A. Safran, Science **290**, 1328 (2000).

[9] V. A. Andreev and A. I. Victorov, Langmuir **22**, 8298 (2006).

[10] A. Karma, in *Branching in Nature* (Springer, Berlin, 2001), chap. XI, pp. 365–401.

[11] P. G. Saffman and G. Taylor, Proc. R. Soc. Lond. A **245**, 312 (1958).

[12] T. Haxhimali *et al.*, Nat. Mater. **5**, 660 (2006).

[13] L. Q. Chen, Annu. Rev. Mater. Res. **32**, 113 (2002).

[14] M. Tang, Ph.D. thesis, MIT (2008).

[15] G. Gompper and M. Schick, Phys. Rev. Lett. **65**, 1116 (1990); G. Gompper and S. Zschocke, Phys. Rev. A **46**, 4836 (1992).

[16] K. R. Elder *et al.*, Phys. Rev. Lett. **88**, 245701 (2002).

[17] J. W. Cahn and J. E. Hilliard, J. Chem. Phys. **28**, 258 (1958).

[18] W. W. Mullins and R. F. Sekerka, J. Appl. Phys. **34**, 323 (1963).

[19] R. W. Balluffi, S. M. Allen, and W. C. Carter, *Kinetics of Materials* (Wiley, New York, 2005).